ACS APPLIED MATERIALS & INTERFACES

Research Article

www.acsami.org

# High Performance PbS Quantum Dot/Graphene Hybrid Solar Cell with Efficient Charge Extraction

Byung-Sung Kim,[†] Darren C. J. Neo,[‡] Bo Hou,[†] Jong Bae Park,[†,§] Yuljae Cho,[†] Nanlin Zhang,[‡] John Hong,[†] Sangyeon Pak,[†] Sanghyo Lee,[†] Jung Inn Sohn,[†] Hazel E. Assender,[‡] Andrew A. R. Watt,*[,‡] SeungNam Cha,*[,†] and Jong Min Kim[⊥]

[†]Department of Engineering Science, University of Oxford, Parks Road, Oxford OX1 3PJ, U.K.

[‡]Department of Materials, University of Oxford, Parks Road, Oxford OX1 3PH, U.K.

[§]Jeonju Centre, Korea Basic Science Institute, Jeonju, Jeollabuk-do 561-180, Republic of Korea

[⊥]Department of Engineering, University of Cambridge, 9 JJ Thomson Avenue, Cambridge CB3 0FA, U.K.

Supporting Information

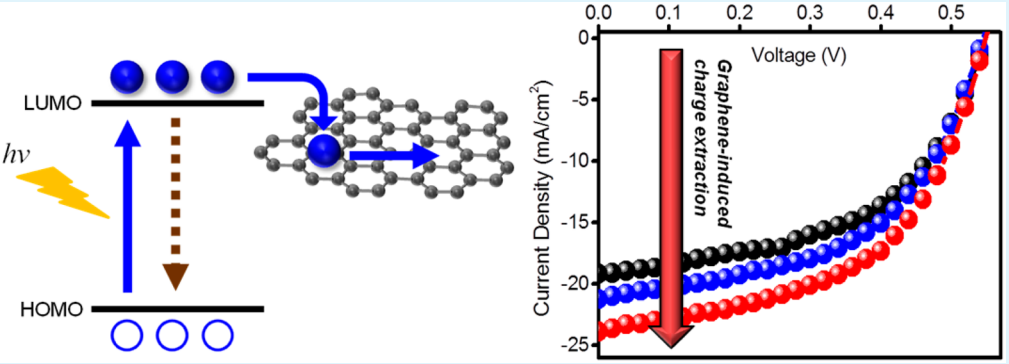


**ABSTRACT:** Hybrid colloidal quantum dot (CQD) solar cells are fabricated from multilayer stacks of lead sulfide (PbS) CQD and single layer graphene (SG). The inclusion of graphene interlayers is shown to increase power conversion efficiency by 9.18%. It is shown that the inclusion of conductive graphene enhances charge extraction in devices. Photoluminescence shows that graphene quenches emission from the quantum dot suggesting spontaneous charge transfer to graphene. CQD photodetectors exhibit increased photoresponse and improved transport properties. We propose that the CQD/SG hybrid structure is a route to make CQD thin films with improved charge extraction, therefore resulting in improved solar cell efficiency.

**KEYWORDS:** *Hybrid solar cell, PbS quantum dot, Graphene, Exciton dissociation, Charge transfer*

## 1. INTRODUCTION

Colloidal quantum dots (CQDs) are known to have outstanding optical and electrical properties, which has led to extensive studies of next generation optoelectronic devices such as light emitting diode, photodetectors, field effect transistors, and photovoltaics.[1−7] In particular, the CQD's tunable bandgap has the potential to cover the entire solar spectrum and harness photon energies more efficiently compared to conventional solar cell.[8−10] To date, device efficiency improvements have been achieved by surface ligand engineering, substitution doping and/or multijunction device architectures.[11−15] To further improve the performance of CQD solar cells, the field has focused on the efficient extraction and transport of photogenerated charge carriers under incident light illumination through the fabrication of favorable energy band alignment of heterojunctions by surface functionalization[16−18] and/or the introduction of hybrid structures with CQD and nano carbon materials.[19−21] However, in spite of these rapid advances in device performance, the cell efficiency still lags behind other emerging solar cell technologies. Herein, we demonstrate a graphene/lead sulfide (PbS) CQD hybrid solar cell that shows enhanced photovoltaic performance dependent on the number of graphene injection layers. The hybrid solar cell is fabricated under ambient condition and graphene layers are inserted between CQD layers via a layer-by-layer deposition method. Furthermore, by employing various analytical techniques, graphene promoted exciton dissociation and improved charge transport in photoexcited PbS are hypothesized to be the origin of this efficiency enhancement.

## 2. EXPERIMENTAL DETAILS

**2.1. Preparation of Colloidal Lead Sulfide Quantum Dots (PbS QDs).**[22,23] Lead precursor was formed by dissolving 2 mmol of lead oxide (PbO) into 6 mmol oleic acid (OA) and 12.7 mL 1-

Received: February 29, 2016
Accepted: May 13, 2016
Published: May 23, 2016

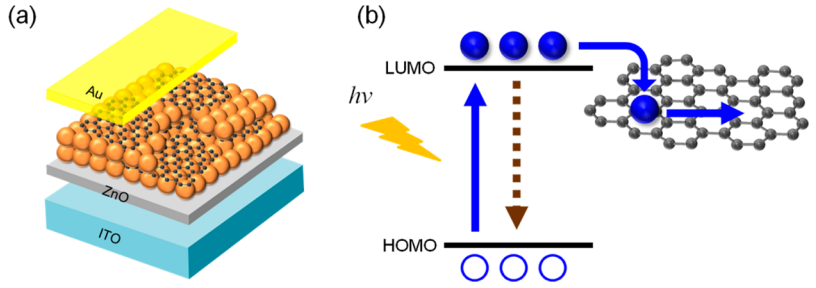


**Figure 1.** Schematic of (a) hybrid solar cell of graphene and semiconductor nanocrystals and (b) electron-transfer interaction. Brown dotted and blue solid arrows indicate recombination in QD and charge transfer from QD to graphene under light illumination, respectively.

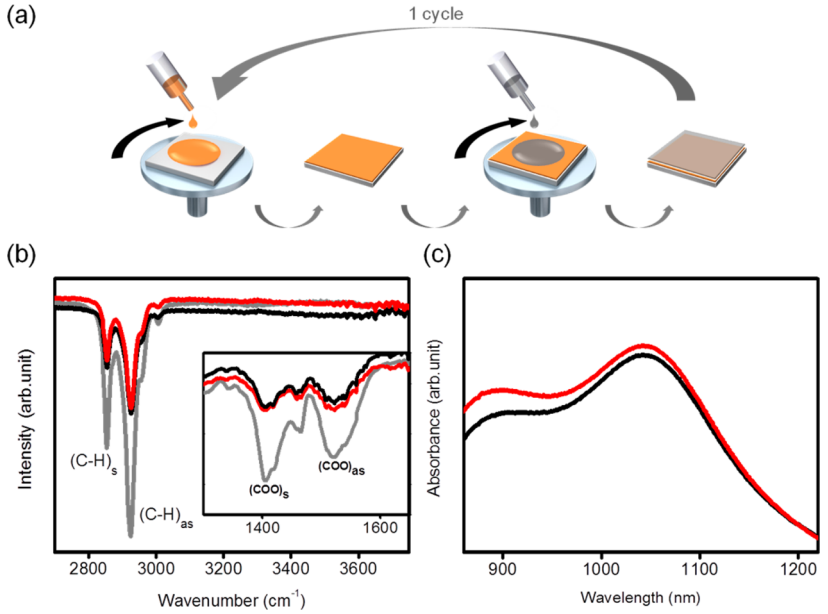


**Figure 2.** (a) Schematic illustrating the fabrication of a layered hybrid structure by using layer-by-layer deposition process. (b) FTIR spectrum of oleic acid-capped (gray solid line), iodide-passivated PbS (black solid line), and iodide-passivated PbS/SG structure (red solid line). (c) UV−Vis absorption spectra of iodide-passivated PbS (black solid line) and PbS/SG (red solid line) structure.

octadecene (ODE), the solution was kept at 100 °C under vacuum for 2 h. Under inert atmosphere, sulfur precursor (hexamethyldisilathiane in 6 mL of ODE) was hot-injected into the lead precursor. The system was subsequently allowed to cool down gradually to room temperature. The PbS QDs were purified several times by dissolving in hexane and precipitating with ethanol. Finally, the precipitation of PbS QDs was dispersed into toluene with a concentration of 50 mg/mL.

**2.2. Preparation of Zinc Oxide Nanoparticles (ZnO NPs) and Single Layer Graphene (SG) Solutions.**[16] Zinc acetate dihydrate (0.9788 g) was dissolved in 42 mL of methanol and heated to 60 °C. Potassium hydroxide (KOH, 0.469 g) was dissolved in 22 mL of methanol and dropped into the reaction flask over a period of 20 min. The solution was kept at 60 °C and the reaction solution turned into transparent pale. Subsequently, the flask was cooled to room temperature. The ZnO nanocrystals were purified and redispersed into methanol. After several purification steps, the ZnO NPs were dispersed into chloroform with a concentration of 50 mg/mL. SG solution was purchased from Graphene Supermarket and highly diluted with ethanol to 1 mg/mL. The average size of the single layered graphene (SG) flake is about 500 nm.

**2.3. Characterization of Semiconductor Quantum Dots and Graphene.** The crystal structure of PbS nanocrystal was characterized by X-ray diffraction (XRD. Bruker D5000) in a two theta range of 10−90°. Transmission electron microscopy (TEM) measurement was carried out on a JEOL JEM-2200MCO FEGTEM. TEM sample was prepared by dropping diluted PbS solution on nickel grid with carbon supporting film. Morphology investigations of PbS and PbS/SG film were measured by scanning electron microscope (SEM, FEI Quanta 600 FEG) and atomic force microscopy (AFM, Veeco Dimension 3100). Fourier transform infrared spectroscopy (FTIR, Varian Excalibur FTS 3500) measurement was performed to confirm the TBAI-ligand exchanged PbS and PbS/SG film on glass substrates. Structural study of single layer graphene was carried out using Raman spectrometer (Horiba Scientific Lab RAM ARAMIS) with 532 nm line for excitation source and UV−visible spectrometer (Varian Cary 5000) with diluted PbS solution in a quartz cuvette. Photoluminescence (PL) quenching behavior was observed using a stationary microphotoluminescence (PL, Horiba LabRam80) spectrum with a 325 nm He−Cd laser (30 mW) as an excitation source at room temperature.

**2.4. Device Fabrication and Measurement (CQD Solar Cell).** The ZnO layer serving as electron-transporting/hole blocking layer was fabricated by spin-coating a solution of ZnO nanoparticles onto patterned ITO/glass substrates. Subsequently, PbS CQD and SG flake layers were prepared by layer-by-layer spin coating at 2000 rpm for 30 s. For the solid-state ligand exchange of PbS layer, tetrabutylammonium iodide solution with concentration of 10 mg/mL was then applied for 30 s when PbS film was held stationary, followed by a two-cycle washing process with methanol. One to two drops of SG solution was deposited onto the PbS surface and the substrate was subsequently washed with methanol and ethanol. 1,2-Ethanedithiol (EDT) solution (0.02 vol% in acetonitrile) was used for electron blocking/hole transport layer in a junction solar cell. All processes were repeated until the desired film thickness had been achieved under ambient condition. Gold (Au) film with 100 nm thickness was deposited by


DOI: 10.1021/acsami.6b02544
ACS Appl. Mater. Interfaces 2016, 8, 13902−13908

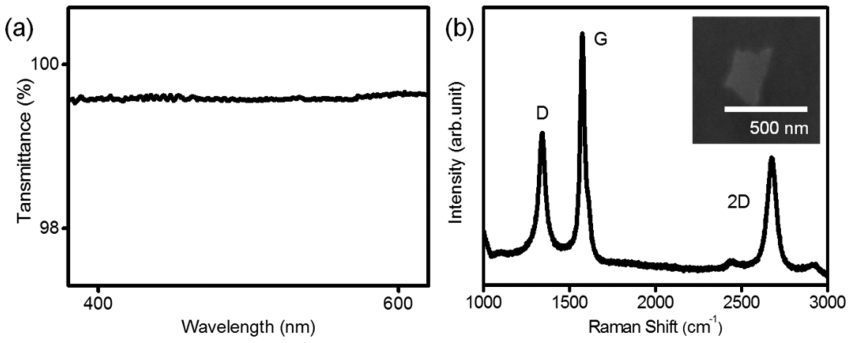


**Figure 3.** (a) Transmittance spectrum and (b) Raman spectrum of the SG flake layer. Inset is a FESEM image of SG flake on PbS QD film surface.

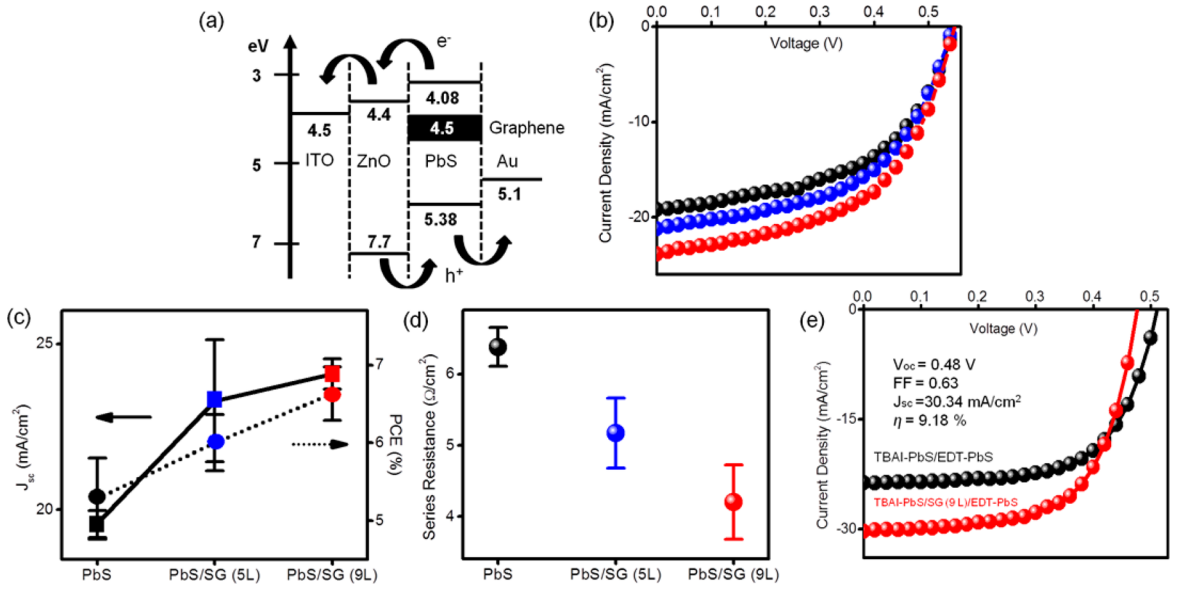


**Figure 4.** (a) Energy level diagram of layered hybrid QD solar cell with graphene. (b) Representative $J-V$ characteristics of the devices under AM 1.5G irradiation at an incident intensity of 100 mW/cm$^2$. Black, blue, and red dotted lines indicate TBAI-PbS, TBAI-PbS/SG (5 layers), and TBAI-PbS/SG (9 layers) devices, respectively. (c and d) Plots of $J_{sc}$, PCE, and $R_s$ of PbS solar cell as a function of graphene injection number. Circle and square in c exhibit $J_{sc}$ and PCE, respectively. (e) $J-V$ characteristics of the devices of TBAI-PbS/EDT-PbS (black dotted line) and TBAI-PbS/SG (9 layers)/EDT-PbS (red dotted line) under illumination with the sun spectrum.

thermal evaporation in high vacuum. A shadow mask was used to define three separated areas of 0.0128 cm$^2$. Solar cell measurements were performed using a source meter (Keithley 4200-SCS) and a solar simulator (LOT-Quantum Design) with an AM 1.5 G filter (100 mW/cm$^2$). The measurement was performed in ambient air at room temperature and confirmed with a certified monocrystalline silicon reference cell (Rera system).

**2.5. Device Fabrication and Measurement (CQD Photodetector).** CQD photodetectors were fabricated using PbS and SG solutions by standard photo lithography process. Photoresist (MICROPOSIT S1813) was spin coated on a heavily doped $p^{++2}$ silicon (100) wafer with a thermally grown 300 nm $SiO_2$ layer and baked at 115 °C for 60 s. The substrate was exposed through a complementary photomask of the electrode pattern and then developed in MICROPOSIT MF-319 developer for 30 s, rinsed in water for 2 min. A metal electrode of 100 nm Au was deposited by thermal evaporation in high vacuum. After lift-off process, PbS and SG solutions are dispersed onto the devices by a layer-by-layer spin coating method. This was repeated for three cycles until the desired shell thickness of approximately 90 nm was reached. Photoresponse measurement was performed in ambient air using a probe station (Cascade Microtech) and Keithley 4200-SCS system.

## 3. RESULTS AND DISCUSSION

Considering the relatively low conductivity of CQDs,[24−26] an intermediate pathway to quickly extract and transfer the photogenerated charge carriers is highly desirable to suppress exciton radiative recombination in the light-absorbing CQD layer. A number of conductive and semiconductive carbon-based materials such as fullerenes and carbon nanotubes have been demonstrated as efficient charge acceptor and/or transport layer in various optoelectronic semiconductor devices.[27−31] Among these functional nano carbon structures for efficient charge dissociation, graphene is one of the most promising candidates because of the lower energy level of graphene to the LUMO of PbS, extremely high electronic mobility ($10^4$ cm$^2$/V·s at room temperature) as well as high transparency due to its atomic thickness (optical absorption of 2.3% per layer) minimizing interruption of the incident light absorption by the QDs.[32,33] Here we use SG flakes as an interlayer as illustrated in Figure 1a. The graphene layer inserted between CQD layers enables efficient extraction and transfer of photoinduced electron from QD to the adjacent graphene due to its high carrier mobility and lower energy level to the LUMO of PbS (Figure 1b).


DOI: 10.1021/acsami.6b02544
ACS Appl. Mater. Interfaces 2016, 8, 13902−13908

**Table 1. Photovoltaic Characteristics of PbS, PbS/SG (5L), and PbS/SG (9L) Solar Cells**[a]

| | $V_{oc}$ (V) | FF | $J_{sc}$ (mA/cm$^2$) | $R_s$ (Ω) | PCE (%) |
|---|---|---|---|---|---|
| PbS | 0.52 ± 0.02 | 0.51 ± 0.02 | 19.58 ± 0.40 | 6.38 ± 0.27 | 5.28 ± 0.53 |
| PbS/SG (5L) | 0.52 ± 0.01 | 0.49 ± 0.01 | 23.28 ± 1.83 | 5.17 ± 0.49 | 6.00 ± 0.36 |
| PbS/SG (9L) | 0.54 ± 0.01 | 0.51 ± 0.02 | 24.09 ± 0.46 | 4.20 ± 0.52 | 6.36 ± 0.34 |

[a]Average values of each device with standard deviations were collected from more than 5 devices.

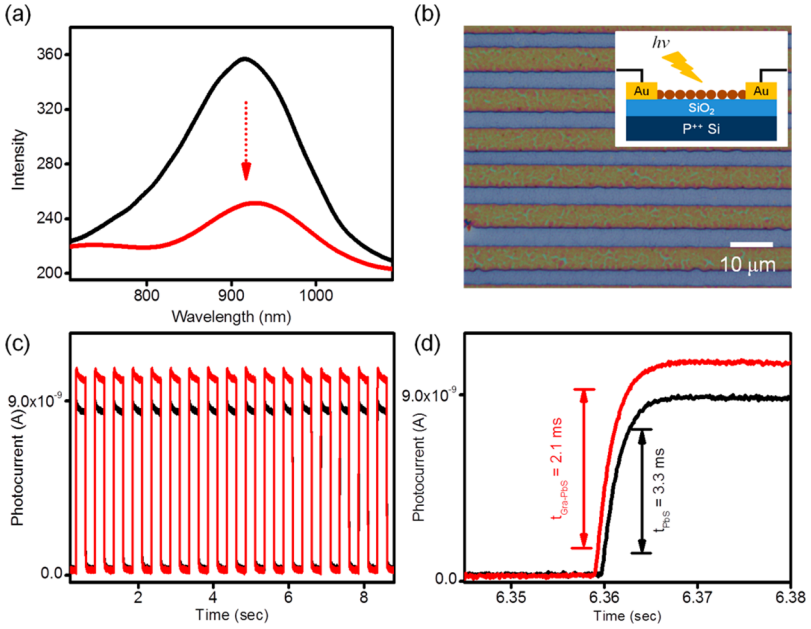


**Figure 5.** (a) Room-temperature PL spectra collected from the 1.37 eV PbS (black solid line) and hybrid PbS/SG structures (red solid line). (b) Optical image of a photodetector device and (c) transient photocurrent characteristics obtained from the 1.3 eV PbS (black solid line) and hybrid PbS/SG structures (red solid line) versus time profiles. Inset of b shows a schematic illustration of photodetector devices. (d) Photoresponse speeds of PbS and PbS/SG devices at a bias 10 V and an incident light density of 4.5 mW/cm$^2$. The photocurrent and rise time ($\tau$) were measured under illumination of a 450 nm laser. The channel length is 5 $\mu$m with Au electrode deposited on 300 nm $SiO_2$/Si substrate.

Generally, as-grown CQDs are passivated by long chain ligands such as oleic acid to prevent the oxidation and the aggregation of the nanocrystals. The ligand exchange from the long chain ligands to shorter chain is an essential processes for CQD-based electronic and optoelectronic devices to increase charge carrier mobility. Layer-by-layer spin coating process (Figure 2a) facilitates the effective ligand exchange of PbS CQD surface compared to the deposition method of CQD/carbon mixed material,[34−36] in which effective ligand exchange of CQDs can be hindered by the carbon materials covering the CQDs but also enables the deposition of SG flake layers with a uniform distribution (Supporting Information Figure S1). Moreover, it can provide a better way to control the number and position of the SG flake layers, resulting in exciton dissociation and charge transport enhancement in the PbS CQD absorption layer. Recently, tetrabutylammonium iodide (TBAI) has been used as an air stable exchange ligand to produce high efficiency photovoltaic devices.[14,37,38] To determine successful ligand exchange in hybrid structure, FTIR spectroscopy was used. Significant reduction of OA related vibrations at 2920 cm$^{-1}$ (asymmetric C−H), 2850 cm$^{-1}$ (symmetric C−H), 1545 cm$^{-1}$ (asymmetric COO−), and 1403 cm$^{-1}$ (symmetric COO−) is observed in the FTIR spectrum of Figure 2b after the ligand exchange process from OA to TBAI. These reduced vibration intensities indicate the removal of OA after iodide passivation and successful ligand exchange through the layer-by-layer deposition for PbS/SG hybrid structure. Both the absorption spectra of 1.3 eV PbS and PbS/SG film structures passivated with the iodide ligand in Figure 2c show a red-shift in absorption (approximately 1020 nm) compared to that of as-grown PbS CQD which is observed in a number of previous reports (Supporting Information Figure S2 and S3)[39−43]

It is known that graphene has outstanding electrical properties, but each layer absorbs a rather large 2.3% of incident light over the visible spectrum. Therefore, use of a diluted SG solution could minimize light absorption while providing considerable electrical pathways even in thick CQD structure. The transmittance of the graphene flake (shown in Figure 3a) is only slightly higher than continuously grown single-layer graphene which means that the light absorption properties of PbS CQD is rarely affected by inserted SG layers. Figure 3b exhibits Raman spectra obtained from the SG flake on $SiO_2$/Si wafer. Three intensive features associated with sp$^2$-bonded graphene were observed at 1341, 1574, and 2677 cm$^{-1}$, corresponding to D band, G band, and 2D band, respectively.[44] The relatively large D peak may be mainly due to the smaller size of SG flakes than the laser spot size of Raman equipment. (inset of Figure 3b).[45,46]

Enhanced performance of the hybrid solar cell through controlled insertion of conductive graphene between TBAI-passivated PbS CQD layers are shown in Figure 4. The devices were prepared by 12 cycle spin coating of PbS on ZnO/ITO substrates with 0, 5, and 9 layers of SG flake (Figure 4a and


DOI: 10.1021/acsami.6b02544
ACS Appl. Mater. Interfaces 2016, 8, 13902−13908

Supporting Information Figure S4).[19] Similar values of the open circuit voltage ($V_{oc}$) were obtained from CQD solar cell with and without graphene interlayers (Table 1). This implies the controlled insertion of SG flakes has no significant influence on the band alignment and interface properties of the solar cell components. However, it is notable that the graphene injection into CQD layers led to a substantial increase of the short-circuit current density ($J_{sc}$) which in turn resulted in high solar efficiency up to 6.99% (Figure 4b and 4c). The performance also depends on the number of the graphene injection layers in the hybrid solar cells. Photogenerated electrons are transferred to the neighboring graphene resulting in a suppression of exciton recombination in the QD, allowing for more efficient collection to the electrodes. The fast charge transport significantly promotes the flow of charge carriers along the absorption layer. This is also supported by the decrease in internal series resistance ($R_s$) as increase of SG layers (Figure 4d). Consistent with $J_{sc}$ and PCE, the $R_s$ values are decreased with graphene injection which enables to provide considerable number of the pathways to overcome the relatively low conductivity of CQD film. The method is now optimized to produce high-efficiency devices. Graphene incorporation in conventional TBAI-PbS/EDT-PbS junction structure results the significantly enhanced photovoltaic performance of 8.82 ± 0.55% with a 9.18% lab champion device. (Figure 4e and Table S1) The devices consisted of 10 layers of TBAI-PbS and 2 layers of EDT-PbS deposited on ZnO/ITO/glass substrates. In the device, 9 layers of SG flake were incorporated in the TBAI-PbS CQD absorber layers. (Supporting Information Figure S5)

The enhanced performance of the PbS/SG hybrid structure due to the fast charge extraction phenomenon is also supported by photoluminescence (PL) quenching behavior under excitation at 325 nm. PL measurement was performed by spin coating 1.37 eV PbS QDs solution onto the glass substrate. The PL spectra both of the PbS and PbS/SG hybrid structures are shown in Figure 5a. All spectra present a dominant broad emission at around 900 nm, which is attributed to the 1.37 eV PbS QDs. However, we noted that the emission intensity of the hybrid structure was dramatically quenched compared to that of PbS one. Taking account of the lower energy level, electron transfer from photoexcited PbS to graphene is energetically favorable. Therefore, the emission quenching in the hybrid structure can be inferred by the enhanced transfer of excited state electron from LUMO of PbS to graphene, while it minimizes charge recombination rate.[47−49]

The fast charge transfer caused by the SG flake in PbS also improves CQD photodetector devices. Figure 5b and 5c show the time-resolved photoresponse of the PbS and hybrid PbS/SG structures upon light illumination. At a fixed bias of 10 V, reproducible photocurrent was obtained by switching repeated on−off cycles of the light irradiation.[50] The photocurrent of the hybrid structure dramatically increases from 272 pA (off state) to 10.6 nA (on state) and the on−off ratio is approximately 1.4 times higher than the PbS device. (Supporting Information Table S2) Moreover, the rise time ($\tau$) of the photoresponse obtained from the PbS/SG device was approximately 2.1 ms, which is faster than the rise time of 3.1 ms in the case of PbS only (Figure 5d). This is attributed to a strong photoexcited state interaction between PbS and the SG flake which leads to the rapidly increasing the flow of charge carriers in the hybrid structure.

## 4. CONCLUSION

In summary, we have fabricated and evaluated hybrid CQD solar cells stacked with graphene layers for efficient charge carrier transfer based on a cost-effective and reliable layer-by-layer deposition process. The photovoltaic performance of the layer-by-layer architecture has shown the enhanced current density from approximately 19.58 ± 0.40 mA/cm$^2$ to 24.09 ± 0.46 mA/cm$^2$ due to the efficient extraction and transportation of photogenerated charges. These phenomena have been examined and supported by the quenching of PL intensity and enhanced photoresponse characteristics leading a high performance of CQD photovoltaic device.

## ■ ASSOCIATED CONTENT

### Supporting Information

The Supporting Information is available free of charge on the ACS Publications website at DOI: 10.1021/acsami.6b02544.

Structural and morphological analysis of PbS QD and SG, photovoltaic performance of TBAI-PbS/EDT-PbS and TBAI-PbS/SG/EDT-PbS junction solar cells. Photoresponse characteristics of PbS and PbS/SG devices (PDF)

## ■ AUTHOR INFORMATION


### Corresponding Authors

* E-mail: andrew.watt@materials.ox.ac.uk.
*E-mail: seungnam.cha@eng.ox.ac.uk.


### Notes

The authors declare no competing financial interest.

## ■ ACKNOWLEDGMENTS

The research leading to these results has received funding from the European Research Council under ERC Grant Agreement n. 340538. The authors would like to thank the financial support from the National Research Foundation (NRF) of Korea (2015M2A2A6A02045252).

## ■ REFERENCES


(1) Caruge, J. M.; Halpert, J. E.; Wood, V.; Bulovic, V.; Bawendi, M. G. Colloidal Quantum-Dot Light-Emitting Diodes with Metal-Oxide Charge Transport Layers. *Nat. Photonics* **2008**, *2*, 247−250.

(2) Zhao, J.; Bardecker, J. A.; Munro, A. M.; Liu, M. S.; Niu, Y.; Ding, I. K.; Luo, J.; Chen, B.; Jen, A. K. Y.; Ginger, D. S. Efficient CdSe/CdS Quantum Dot Light-Emitting Diodes using a Thermally Polymerized Hole Transport Layer. *Nano Lett.* **2006**, *6*, 463−467.

(3) Dai, X.; Zhang, Z.; Jin, Y.; Niu, Y.; Cao, H.; Liang, X.; Chen, L.; Wang, J.; Peng, X. Solution-Processed, High-Performance Light-Emitting Diodes based on Quantum Dots. *Nature* **2014**, *515*, 96−99.

(4) Konstantatos, G.; Howard, I.; Fischer, A.; Hoogland, S.; Clifford, J.; Klem, E.; Levina, L.; Sargent, E. H. Ultrasensitive Solution-Cast Quantum Dot Photodetectors. *Nature* **2006**, *442*, 180−183.

(5) Prins, F.; Buscema, M.; Seldenthuis, J. S.; Etaki, S.; Buchs, G.; Barkelid, M.; Zwiller, V.; Gao, Y.; Houtepen, A. J.; Siebbeles, L. D. A.; Van Der Zant, H. S. J. Fast and Efficient Photodetection in Nanoscale Quantum-Dot Junctions. *Nano Lett.* **2012**, *12*, 5740−5743.

(6) Liu, Y.; Tolentino, J.; Gibbs, M.; Ihly, R.; Perkins, C. L.; Liu, Y.; Crawford, N.; Hemminger, J. C.; Law, M. PbSe Quantum Dot Field-Effect Transistors with Air-Stable Electron Mobilities above 7 cm$^2$ V$^{-1}$ s$^{-1}$. *Nano Lett.* **2013**, *13*, 1578−1587.

(7) Ghosh, S.; Hoogland, S.; Sukhovatkin, V.; Levina, L.; Sargent, E. H. A Tunable Colloidal Quantum Dot Photo Field-Effect Transistor. *Appl. Phys. Lett.* **2011**, *99*, 101102.

(8) Alivisatos, A. P. Semiconductor Clusters, Nanocrystals, and Quantum Dots. *Science* **1996**, *271*, 933−937.




DOI: 10.1021/acsami.6b02544
*ACS Appl. Mater. Interfaces* 2016, 8, 13902−13908

(9) Kang, Z.; Liu, Y.; Tsang, C. H. A.; Ma, D. D. D.; Fan, X.; Wong, N. B.; Lee, S. T. Water-Soluble Silicon Quantum Dots with Wavelength-Tunable Photoluminescence. *Adv. Mater.* **2009**, *21*, 661−664.
(10) Ruddy, D. A.; Johnson, J. C.; Smith, E. R.; Neale, N. R. Size and Bandgap Control in the Solution-Phase Synthesis of Near-Infrared-Emitting Germanium Nanocrystals. *ACS Nano* **2010**, *4*, 7459−7466.
(11) Dubois, F.; Mahler, B.; Dubertret, B.; Doris, E.; Mioskowski, C. A Versatile Strategy for Quantum Dot Ligand Exchange. *J. Am. Chem. Soc.* **2007**, *129*, 482−483.
(12) Zillner, E.; Fengler, S.; Niyamakom, P.; Rauscher, F.; Köhler, K.; Dittrich, T. Role of Ligand Exchange at CdSe Quantum Dot Layers for Charge Separation. *J. Phys. Chem. C* **2012**, *116*, 16747−16754.
(13) Brown, P. R.; Kim, D.; Lunt, R. R.; Zhao, N.; Bawendi, M. G.; Grossman, J. C.; Bulović, V. Energy Level Modification in Lead Sulfide Quantum Dot Thin Films through Ligand Exchange. *ACS Nano* **2014**, *8*, 5863−5872.
(14) Tang, J.; Kemp, K. W.; Hoogland, S.; Jeong, K. S.; Liu, H.; Levina, L.; Furukawa, M.; Wang, X.; Debnath, R.; Cha, D.; Chou, K. W.; Fischer, A.; Amassian, A.; Asbury, J. B.; Sargent, E. H. Colloidal-Quantum-Dot Photovoltaics using Atomic-Ligand Passivation. *Nat. Mater.* **2011**, *10*, 765−771.
(15) Stavrinadis, A.; Rath, A. K.; de Arquer, F. P. G.; Diedenhofen, S. L.; Magén, C.; Martinez, L.; So, D.; Konstantatos, G. Heterovalent Cation Substitutional Doping for Quantum Dot Homojunction Solar Cells. *Nat. Commun.* **2013**, *4*, 2981.
(16) Chuang, C. H. M.; Brown, P. R.; Bulović, V.; Bawendi, M. G. Improved Performance and Stability in Quantum Dot Solar Cells through Band Alignment Engineering. *Nat. Mater.* **2014**, *13*, 796−801.
(17) Lan, X.; Masala, S.; Sargent, E. H. Charge-Extraction Strategies for Colloidal Quantum Dot Photovoltaics. *Nat. Mater.* **2014**, *13*, 233−240.
(18) Ko, D. K.; Brown, P. R.; Bawendi, M. G.; Bulovic, V. P-I-N Heterojunction Solar Cells with a Colloidal Quantum-dot Absorber Layer. *Adv. Mater.* **2014**, *26*, 4845−4850.
(19) Hu, L.; Li, D. B.; Gao, L.; Tan, H.; Chen, C.; Li, K.; Li, M.; Han, J. B.; Song, H.; Liu, H.; Tang, J. Graphene Doping Improved Device Performance of ZnMgO/PbS Colloidal Quantum Dot Photovoltaics. *Adv. Funct. Mater.* **2016**, *26*, 1899−1907.
(20) Guo, C. X.; Yang, H. B.; Sheng, Z. M.; Lu, Z. S.; Song, Q. L.; Li, C. M. Layered Graphene/Quantum dots for Photovoltaic Devices. *Angew. Chem., Int. Ed.* **2010**, *49*, 3014−3017.
(21) Meng, W.; Zhou, X.; Qiu, Z.; Liu, C.; Chen, J.; Yue, W.; Wang, M.; Bi, H. Reduced Graphene Oxide-Supported Aggregates of $CuInS_2$ Quantum Dots as an Effective Hybrid Electron Acceptor for Polymer-based Solar cells. *Carbon* **2016**, *96*, 532−540.
(22) Hines, M. A.; Scholes, G. D. Colloidal PbS Nanocrystals with Size-Tunable Near-Infrared Emission: Observation of Post-Synthesis Self-Narrowing of the Particle Size Distribution. *Adv. Mater.* **2003**, *15*, 1844−1849.
(23) Barkhouse, D. A. R.; Debnath, R.; Kramer, I. J.; Zhitomirsky, D.; Pattantyus-Abraham, A. G.; Levina, L.; Etgar, L.; Grätzel, M.; Sargent, E. H. Depleted Bulk Heterojunction Colloidal Quantum Dot Photovoltaics. *Adv. Mater.* **2011**, *23*, 3134−3138.
(24) Meir, Y.; Wingreen, N. S.; Lee, P. A. Low-Temperature Transport through a Quantum Dot: The Anderson Model out of Equilibrium. *Phys. Rev. Lett.* **1993**, *70*, 2601−2604.
(25) Kunets, V. P.; Dias, M. R. S.; Rembert, T.; Ware, M. E.; Mazur, Y. I.; Lopez-Richard, V.; Mantooth, H. A.; Marques, G. E.; Salamo, G. J. Electron Transport in Quantum Dot Chains: Dimensionality Effects and Hopping Conductance. *J. Appl. Phys.* **2013**, *113*, 183709.
(26) Wingreen, N. S.; Meir, Y. Anderson Model out of Equilibrium: Noncrossing-Approximation Approach to Transport through a Quantum Dot. *Phys. Rev. B: Condens. Matter Mater. Phys.* **1994**, *49*, 11040−11052.
(27) Thompson, B. C.; Fréchet, J. M. J. Polymer-Fullerene Composite Solar Cells. *Angew. Chem., Int. Ed.* **2008**, *47*, 58−77.
(28) Lee, J. M.; Kwon, B. H.; Park, H. I.; Kim, H.; Kim, M. G.; Park, J. S.; Kim, E. S.; Yoo, S.; Jeon, D. Y.; Kim, S. O. Exciton Dissociation and Charge-Transport Enhancement in Organic Solar Cells with Quantum-Dot/N-doped CNT Hybrid Nanomaterials. *Adv. Mater.* **2013**, *25*, 2011−2017.
(29) Kymakis, E.; Alexandrou, I.; Amaratunga, G. A. J. High Open-Circuit Voltage Photovoltaic Devices from Carbon-Nanotube-Polymer Composites. *J. Appl. Phys.* **2003**, *93*, 1764−1768.
(30) Guldi, D. M.; Rahman, G. M. A.; Zerbetto, F.; Prato, M. Carbon Nanotubes in Electron Donor - Acceptor Nanocomposites. *Acc. Chem. Res.* **2005**, *38*, 871−878.
(31) Jun, G. H.; Jin, S. H.; Lee, B.; Kim, B. H.; Chae, W. S.; Hong, S. H.; Jeon, S. Enhanced Conduction and Charge-Selectivity by N-doped Graphene Flakes in the Active Layer of Bulk-Heterojunction Organic Solar Cells. *Energy Environ. Sci.* **2013**, *6*, 3000−3006.
(32) Nair, R. R.; Blake, P.; Grigorenko, A. N.; Novoselov, K. S.; Booth, T. J.; Stauber, T.; Peres, N. M. R.; Geim, A. K. Fine Structure Constant Defines Visual Transparency of Graphene. *Science* **2008**, *320*, 1308.
(33) Bolotin, K. I.; Sikes, K. J.; Jiang, Z.; Klima, M.; Fudenberg, G.; Hone, J.; Kim, P.; Stormer, H. L. Ultrahigh Electron Mobility in Suspended Graphene. *Solid State Commun.* **2008**, *146*, 351−355.
(34) Yuan, L.; Jiang, L.; Liu, J.; Xia, Z.; Wang, S.; Sun, G. Facile Synthesis of Silver Nanoparticles Supported on Three Dimensional Graphene Oxide/Carbon Black Composite and Its Application for Oxygen Reduction Reaction. *Electrochim. Acta* **2014**, *135*, 168−174.
(35) Markad, G. B.; Battu, S.; Kapoor, S.; Haram, S. K. Interaction Between Quantum Dots of CdTe and Reduced Graphene Oxide: Investigation through Cyclic Voltammetry and Spectroscopy. *J. Phys. Chem. C* **2013**, *117*, 20944−20950.
(36) Banerjee, S.; Wong, S. S. In situ Quantum Dot Growth on Multiwalled Carbon Nanotubes. *J. Am. Chem. Soc.* **2003**, *125*, 10342−10350.
(37) Ning, Z.; Voznyy, O.; Pan, J.; Hoogland, S.; Adinolfi, V.; Xu, J.; Li, M.; Kirmani, A. R.; Sun, J. P.; Minor, J.; Kemp, K. W.; Dong, H.; Rollny, L.; Labelle, A.; Carey, G.; Sutherland, B.; Hill, I.; Amassian, A.; Liu, H.; Tang, J.; Bakr, O. M.; Sargent, E. H. Air-Stable N-Type Colloidal Quantum Dot Solids. *Nat. Mater.* **2014**, *13*, 822−828.
(38) Milliron, D. J. Quantum Dot Solar Cells: The Surface Plays a Core Role. *Nat. Mater.* **2014**, *13*, 772−773.
(39) Ma, W.; Luther, J. M.; Zheng, H.; Wu, Y.; Alivisatos, A. P. Photovoltaic Devices Employing Ternary $PbS_xSe_{1-x}$ Nanocrystals. *Nano Lett.* **2009**, *9*, 1699−1703.
(40) Williams, K. J.; Tisdale, W. A.; Leschkies, K. S.; Haugstad, G.; Norris, D. J.; Aydil, E. S.; Zhu, X. Y. Strong Electronic Coupling in Two-Dimensional Assemblies of Colloidal PbSe Quantum Dots. *ACS Nano* **2009**, *3*, 1532−1538.
(41) Koole, R.; Liljeroth, P.; De Mello Donegá, C.; Vanmaekelbergh, D.; Meijerink, A. Electronic Coupling and Exciton Energy Transfer in CdTe Quantum-Dot Molecules. *J. Am. Chem. Soc.* **2006**, *128*, 10436−10441.
(42) Fafarman, A. T.; Koh, W. K.; Diroll, B. T.; Kim, D. K.; Ko, D. K.; Oh, S. J.; Ye, X.; Doan-Nguyen, V.; Crump, M. R.; Reifsnyder, D. C.; Murray, C. B.; Kagan, C. R. Thiocyanate-Capped Nanocrystal Colloids: Vibrational Reporter of Surface Chemistry and Solution-based Route to Enhanced Coupling in Nanocrystal Solids. *J. Am. Chem. Soc.* **2011**, *133*, 15753−15761.
(43) Zillner, E.; Fengler, S.; Niyamakom, P.; Rauscher, F.; Köhler, K.; Dittrich, T. Role of Ligand Exchange at CdSe Quantum Dot Layers for Charge Separation. *J. Phys. Chem. C* **2012**, *116*, 16747−16754.
(44) Ferrari, A. C.; Meyer, J. C.; Scardaci, V.; Casiraghi, C.; Lazzeri, M.; Mauri, F.; Piscanec, S.; Jiang, D.; Novoselov, K. S.; Roth, S.; Geim, A. K. Raman Spectrum of Graphene and Graphene Layers. *Phys. Rev. Lett.* **2006**, *97*, 187401.
(45) Ferrari, A. C. Raman Spectroscopy of Graphene and Graphite: Disorder, Electron-Phonon Coupling, Doping and Nonadiabatic Effects. *Solid State Commun.* **2007**, *143*, 47−57.
(46) Katagiri, G.; Ishida, H.; Ishitani, A. Raman Spectra of Graphite Edge Planes. *Carbon* **1988**, *26*, 565−571.
(47) Robel, I.; Bunker, B. A.; Kamat, P. V. Single-Walled Carbon Nanotube-CdS Nanocomposites as Light-Harvesting Assemblies:


DOI: 10.1021/acsami.6b02544
*ACS Appl. Mater. Interfaces* 2016, 8, 13902−13908

Photoinduced Charge-Transfer Interactions. *Adv. Mater.* **2005**, *17*, 2458−2463.
(48) Biju, V.; Itoh, T.; Baba, Y.; Ishikawa, M. Quenching of Photoluminescence in Conjugates of Quantum Dots and Single-Walled Carbon Nanotube. *J. Phys. Chem. B* **2006**, *110*, 26068−26074.
(49) Martín-García, B.; Polovitsyn, A.; Prato, M.; Moreels, I. Efficient Charge Transfer in Solution-processed PbS Quantum Dot-Reduced Graphene Oxide Hybrid Materials. *J. Mater. Chem. C* **2015**, *3*, 7088−7095.
(50) Saran, R.; Curry, R. J. Lead Sulphide Nanocrystal Photodetector Technologies. *Nat. Photonics* **2016**, *10*, 81−92.



DOI: 10.1021/acsami.6b02544
*ACS Appl. Mater. Interfaces* 2016, 8, 13902−13908